Disturbance Observer-Based Robust Saturated Control for Spacecraft Proximity Maneuvers

Liang Sun, *Member, IEEE*, and Zewei Zheng, *Member, IEEE*

***Abstract*— The problem of six-degrees-of-freedom (6-DOF) relative motion control is investigated for spacecraft close proximity maneuvers with input saturation and model uncertainties. A nonlinear disturbance observer is developed to estimate the lumped disturbance that comprises the effects of parametric uncertainties, measurement uncertainties, kinematic couplings, and external environment disturbances, while a linear compensator system is incorporated into the controller design to deal with the control input saturation. A 6-DOF robust state feedback saturated controller is designed for relative position tracking and attitude synchronization simultaneously, and the same is augmented by the linear saturation compensator and nonlinear disturbance observer to compensate the control input saturation effect and model uncertainties, respectively. Rigorous stability of the closed-loop system with the proposed control method is established under mild assumptions, and it is proven that the relative position and the relative attitude converge to a small neighborhood of zero. Numerical simulation result demonstrates the effectiveness of the proposed controller designing method.**

***Index Terms*— Close proximity maneuvers, control input saturation, nonlinear disturbance observer, robust control, spacecraft control.**

I. Introduction

AUTONOMOUS spacecraft proximity maneuver is an important technology in many future space missions, such as rendezvous and docking, hovering and capturing, repairing and refueling, and debris removing in orbit. However, the model of spacecraft relative motion, in fulfilling those tasks, is usually subject to uncertain or unmodeled dynamics, even if the mass and inertial parameters of chaser spacecraft are known. These uncertain dynamics always result from the restricts of the actuator outputs, target's uncertain parameters, and unknown motion information, and thus, these effects which are neither negligible nor easy to measure make the motion control of close proximity maneuvers a challenging work.

The design of guidance and control systems for the spacecraft has attracted a great deal of attention in the past few years [1]. Stansbery and Cloutier [2] proposed a robust controller based on state-dependent Riccati equation technology for spacecraft relative position and relative attitude motions. Philip and Ananthasayanam [3] adopted phase plane technique and relative quaternion feedback approach to address the relative position and relative attitude control problem. Subbarao and Welsh [4] developed a feedback-linearization-based position controller and an adaptive state feedback attitude controller for spacecraft proximity operations in the presence of parametric uncertainties, bounded disturbances, and measurement noises. Liang and Ma [5] proposed a Lyapunov-based adaptive tracking control approach to track the angular velocity of a tumbling satellite before docking and stabilize the rotation of the two-satellite compound system after docking. Without considering the relative translational motion, a cooperative attitude tracking controller was studied in [6]. Singla *et al.* [7] designed an adaptive output feedback controller based on the feedback linearization and Lyapunov stability theory considering parametric uncertainties, bounded disturbances, and measurement uncertainties. McCamish *et al.* [8] presented a distributed control algorithm based on linear quadratic regulator and artificial potential function for simultaneous proximity and docking maneuvers of multiple spacecraft, and the numerical simulation was developed through the Monte Carlo analysis. Xin and Pan [9] presented a closed-form nonlinear optimal control solution of spacecraft to approach a target spacecraft by using the θ-D technique. They researched again the problem in [10] and redesigned the optimal controller with considering the modeling uncertainties. The spacecraft relative position control problem was converted into a model predictive control optimization problem in [11] with considering constraints on thrust magnitude and approach velocity. Zhang and Duan [12] formulated a finite-time controller for spacecraft relative motion by designing a predetermined trajectory, and the thruster installation misalignment was also modeled.

Although aforementioned methods have gained extensive applications and been proven to be efficient for spacecraft proximity systems, they mainly focus on the stability of the uncertain spacecraft proximity systems, the input saturation effect is not considered and the robustness is achieved at a price of sacrificing the nominal control performance, and the disturbances are not rejected actively and directly, as a practical alternative to these techniques is the use of the so-called "disturbance observers." In general, the idea behind the disturbance observer is to lump all the internal and external unknown forces and torques acting on the controlled plant into a single disturbance term and then estimate this unknown term using the disturbance observers. The output of the disturbance observer can be used in feedforward compensation of

Manuscript received April 27, 2016; revised September 12, 2016; accepted January 28, 2017. Date of publication March 6, 2017; date of current version February 8, 2018. Manuscript received in final form February 10, 2017. This work was supported in part by the China Postdoctoral Science Foundation under Grant 2016M590031, in part by the Natural Science Foundation of China under Grant 61327807 and Grant 61503010, in part by the Aeronautical Science Foundation of China under Grant 2016ZA51001, and in part by the Fundamental Research Funds for the Central Universities under Grant YWF-16-GJSYS-02. Recommended by Associate Editor K. Morgansen.

The authors are with the Seventh Research Division, Science and Technology on Aircraft Control Laboratory, School of Automation Science and Electrical Engineering, Beihang University, Beijing 100191, China (e-mail: liangsun@buaa.edu.cn; zeweizheng@buaa.edu.cn).

Color versions of one or more of the figures in this paper are available online at http://ieeexplore.ieee.org.

Digital Object Identifier 10.1109/TCST.2017.2669145

unknown disturbances. Disturbance observer has been received a great deal of attention in recent years, due to its simplicity, transparency, and excellent disturbance compensation ability. Chen [13] and Guo and Chen [14] proposed a typically nonlinear disturbance observer for nonlinear systems with matched disturbances and applied it in the missile flight control systems [15]. Then, a novel disturbance-observer-based controller design approach was proposed by Yang *et al.* [16] to deal with the mismatched disturbances in nonlinear systems, and it is shown that the effect of mismatched disturbances can be eliminated from the output by appropriately designing a disturbance compensation gain matrix. This disturbance observer design method was widely applied to many aeronautical engineering to design the robust flight controllers, such as fixed-wing unmanned aerial vehicles [17], missiles [18], and airbreathing hypersonic vehicles [19]. For the spacecraft control systems, Hu *et al.* [20] designed a nonlinear-disturbance-observer-based saturated attitude stabilization controller to reject the lumped disturbances in the attitude dynamics, so that parametric uncertainties, external disturbance, and actuator misalignment were compensated in the closed-loop system. Wu *et al.* [21] presented a sliding mode attitude tracking controller with the aid of disturbance observer to compensate the unknown disturbances and improve the robustness of spacecraft systems. Cong *et al.* [22] proposed an adaptive integral sliding mode attitude maneuver controller augmented with disturbance observer to improve the dynamic performance of traditional sliding mode controller.

The spacecraft proximity maneuvers are essentially multi-input-multioutput nonlinear systems subject to input saturation effect, parametric uncertainties, measurement uncertainties, complicated kinematic couplings, and unknown environmental disturbances, which bring great challenges for the composite controller design via disturbance observer. The significant contributions of this brief are as follows: 1) compared with the decoupled design of relative position and attitude controllers in [3]–[7], relative position and attitude controllers are developed simultaneously based on a disturbance observer, where the upper bounds of lumped disturbances are unknown; 2) compared with the nonlinear controllers in [4]–[12] and our previous studies [23]–[25], the input saturation effect is addressed and compensated by the proposed saturation compensator in the six-degrees-of-freedom (6-DOF) controller design to achieve relative position tracking and attitude synchronization, while the accelerations of the target's position and attitude are avoided in the proposed robust saturated controller; and 3) compared with the disturbance observers for spacecraft control systems in [20]–[22], the proposed disturbance observer can uniformly estimate and compensate the parametric uncertainties, measurement uncertainties, kinematic couplings, and environmental disturbances in the robust controller, while the gains of disturbance observer and controller can be regulated separately under the mild assumptions. It is proven that system tracking errors in closed-loop system keep bounded under suitable observer and controller gains. Effectiveness of the proposed approach is demonstrated through simulation example with significant uncertainties in the system model.

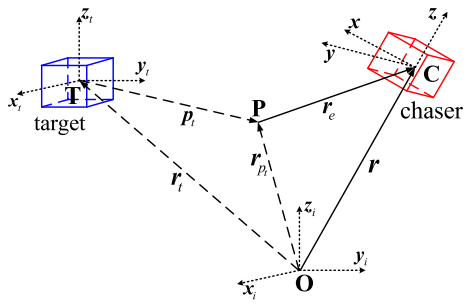

Fig. 1. Definitions of vectors and frames.

The rest of this brief is arranged as follows. In Section II, the mechanical model of the spacecraft proximity maneuvers is derived, and the objective of the controller design is stated. In Section III, an observer and a controller are proposed, and a detailed stability analysis is presented. Simulation results are displayed in Section IV. The conclusion is given in Section V.

II. Problem Description

Notations: The skew-symmetric matrix $S(\boldsymbol{a}) \in \mathbb{R}^{3\times 3}$ for any vector $\boldsymbol{a} = [a_1, a_2, a_3]^T \in \mathbb{R}^3$ is defined by

$$S(\boldsymbol{a}) = \begin{bmatrix} 0 & -a_3 & a_2 \\ a_3 & 0 & -a_1 \\ -a_2 & a_1 & 0 \end{bmatrix}.$$

It satisfies $\boldsymbol{a}^T S(\boldsymbol{a}) = 0$, $\|S(\boldsymbol{a})\| = \|\boldsymbol{a}\|$, and $S(\boldsymbol{a})\boldsymbol{b} = -S(\boldsymbol{b})\boldsymbol{a}$, $\boldsymbol{b}^T S(\boldsymbol{a})\boldsymbol{b} = 0$ for any $\boldsymbol{b} \in \mathbb{R}^3$. $\|\boldsymbol{a}\|$ denotes vector 2-norm of $\boldsymbol{a}$, $\|A\|$ represents the induced matrix 2-norm of A. I_n and O_n are $n \times n$ unit and zero matrices, respectively.

A. Chaser and Target Dynamics

The control problem that a chaser spacecraft tracks a tumbling space target is investigated in this brief. The related frames and vectors are defined in Fig. 1, where $\mathcal{F}_i \triangleq \{\mathbf{O}x_i y_i z_i\}$ is the earth-centered inertial frame, and $\mathcal{F}_c \triangleq \{\mathbf{C}xyz\}$ and $\mathcal{F}_t \triangleq \{\mathbf{T}x_t y_t z_t\}$ are spacecraft body-fixed frames of the chaser and target, respectively; the origins **C** and **T** are the centers of mass of the chaser and target, respectively; point **P** is a fixed point with respect to the target and it is the desired proximity position of the chaser; solid arrows $\{\boldsymbol{r}, \boldsymbol{r}_e\}$ and dashed arrows $\{\boldsymbol{r}_t, \boldsymbol{r}_{p_t}, \boldsymbol{p}_t\}$ are related position vectors expressed in frame $\mathcal{F}_c$ and $\mathcal{F}_t$, respectively. The objective is to control the chaser, such that its center of mass **C** tracks point **P** and frame $\mathcal{F}_c$ tracks frame $\mathcal{F}_t$.

The position of center of mass **C** and the attitude of frame $\mathcal{F}_c$ with respect to frame $\mathcal{F}_i$ can be described by following kinematics and dynamics expressed in frame $\mathcal{F}_c$, if the modified Rodrigues parameters (MRPs) are used for attitude parameterization [26]:

$$\begin{cases} \dot{\boldsymbol{r}} = \boldsymbol{v} - S(\boldsymbol{\omega})\boldsymbol{r} \\ \dot{\boldsymbol{\sigma}} = G(\boldsymbol{\sigma})\boldsymbol{\omega} \\ m\dot{\boldsymbol{v}} + mS(\boldsymbol{\omega})\boldsymbol{v} + m\mu\boldsymbol{r} = \boldsymbol{f} + \boldsymbol{d}_f \\ J\dot{\boldsymbol{\omega}} + S(\boldsymbol{\omega})J\boldsymbol{\omega} = \boldsymbol{\tau} + \boldsymbol{d}_\tau \end{cases} \tag{1}$$

where $G(\boldsymbol{\sigma}) = (1/(4))[(1-\boldsymbol{\sigma}^T\boldsymbol{\sigma})I_3 + 2S(\boldsymbol{\sigma}) + 2\boldsymbol{\sigma}\boldsymbol{\sigma}^T]$; $\mu = \mu_g/\|\boldsymbol{r}\|^3$; $\boldsymbol{r} \in \mathbb{R}^3$ and $\boldsymbol{\sigma}$ are position and MRP attitude of the chaser, respectively; $\boldsymbol{v}, \boldsymbol{\omega} \in \mathbb{R}^3$ are linear and angular velocities, respectively; $\boldsymbol{f}, \boldsymbol{\tau} \in \mathbb{R}^3$ are the control force and torque, respectively; $\boldsymbol{d}_f, \boldsymbol{d}_\tau \in \mathbb{R}^3$ are the disturbance force and torque, respectively; μ_g is the gravitational constant of the earth; $m \in \mathbb{R}$ and $J \in \mathbb{R}^{3\times3}$ are the chaser's mass and the positive definite symmetric inertia matrix, respectively.

Consider the target moves in a circular orbit. With only considering the gravity and ignoring the other external forces and torques, kinematics and dynamics of the free-tumbling target can be described in frame $\mathcal{F}_t$ as [27]

$$\begin{cases} \dot{\boldsymbol{r}}_t = \boldsymbol{v}_t - S(\boldsymbol{\omega}_t)\boldsymbol{r}_t \\ \dot{\boldsymbol{\sigma}}_t = G(\boldsymbol{\sigma}_t)\boldsymbol{\omega}_t \\ m_t\dot{\boldsymbol{v}}_t + m_t S(\boldsymbol{\omega}_t)\boldsymbol{v}_t + m_t\mu_t\boldsymbol{r}_t = \boldsymbol{0} \\ J_t\dot{\boldsymbol{\omega}}_t + S(\boldsymbol{\omega}_t)J_t\boldsymbol{\omega}_t = \boldsymbol{0} \end{cases} \tag{2}$$

where $G(\boldsymbol{\sigma}_t) = (1/(4))[(1-\boldsymbol{\sigma}_t^T\boldsymbol{\sigma}_t)I_3 + 2S(\boldsymbol{\sigma}_t) + 2\boldsymbol{\sigma}_t\boldsymbol{\sigma}_t^T]$; $\mu_t = \mu_g/\|r_o\|^3$, $\boldsymbol{r}_t \in \mathbb{R}^3$ and $\boldsymbol{\sigma}_t$ are position and attitude of the target, respectively; $\boldsymbol{v}_t, \boldsymbol{\omega}_t \in \mathbb{R}^3$ are linear and angular velocities of the target, respectively; r_o is the radius of the circular orbit; $m_t \in \mathbb{R}$ and $J_t \in \mathbb{R}^{3\times3}$ are mass and inertial matrix of the target, respectively.

B. Relative Motion Dynamics

The MRP of relative attitude is defined in frame $\mathcal{F}_c$ by [28]

$$\boldsymbol{\sigma}_e = \frac{\boldsymbol{\sigma}_t(\boldsymbol{\sigma}^T\boldsymbol{\sigma}-1) + \boldsymbol{\sigma}(1-\boldsymbol{\sigma}_t^T\boldsymbol{\sigma}_t) - 2S(\boldsymbol{\sigma}_t)\boldsymbol{\sigma}}{1+\boldsymbol{\sigma}_t^T\boldsymbol{\sigma}_t\boldsymbol{\sigma}^T\boldsymbol{\sigma} + 2\boldsymbol{\sigma}_t^T\boldsymbol{\sigma}} \tag{3}$$

and the corresponding rotation matrix from frame $\mathcal{F}_t$ to frame $\mathcal{F}_c$ is

$$R = I_3 - \frac{4\left(1-\boldsymbol{\sigma}_e^T\boldsymbol{\sigma}_e\right)}{\left(1+\boldsymbol{\sigma}_e^T\boldsymbol{\sigma}_e\right)^2}S(\boldsymbol{\sigma}_e) + \frac{8}{\left(1+\boldsymbol{\sigma}_e^T\boldsymbol{\sigma}_e\right)^2}S^2(\boldsymbol{\sigma}_e). \tag{4}$$

According to Fig. 1, the position and the velocity of point $\mathbf{P}$ represented in frame $\mathcal{F}_t$ can be obtained by

$$\boldsymbol{r}_{p_t} = \boldsymbol{r}_t + \boldsymbol{p}_t, \quad \boldsymbol{v}_{p_t} = \boldsymbol{v}_t + S(\boldsymbol{\omega}_t)\boldsymbol{p}_t \tag{5}$$

where $\boldsymbol{p}_t \in \mathbb{R}^3$ is a constant vector in frame $\mathcal{F}_t$. The relative position, relative linear velocity, and relative angular velocity are described in frame $\mathcal{F}_c$ by

$$\boldsymbol{r}_e = \boldsymbol{r} - R\boldsymbol{r}_{p_t}, \quad \boldsymbol{v}_e = \boldsymbol{v} - R\boldsymbol{v}_{p_t}, \quad \boldsymbol{\omega}_e = \boldsymbol{\omega} - R\boldsymbol{\omega}_t. \tag{6}$$

Substituting (6) into (1) and using the facts $\dot{R} = -S(\boldsymbol{\omega}_e)R$, $\dot{\boldsymbol{r}}_{p_t} = \boldsymbol{v}_{p_t} - S(\boldsymbol{\omega}_t)\boldsymbol{r}_{p_t}$, and $R^{-1} = R^T$ yield the relative motion equations expressed in frame $\mathcal{F}_c$ by [25]

$$\begin{cases} \dot{\boldsymbol{r}}_e = \boldsymbol{v}_e - S(\boldsymbol{\omega})\boldsymbol{r}_e \\ \dot{\boldsymbol{\sigma}}_e = G(\boldsymbol{\sigma}_e)\boldsymbol{\omega}_e \\ m\dot{\boldsymbol{v}}_e = -m(R\dot{\boldsymbol{v}}_{p_t} + \boldsymbol{g}_e) + \boldsymbol{f} + \boldsymbol{d}_f \\ J\dot{\boldsymbol{\omega}}_e = -S(\boldsymbol{\omega})J\boldsymbol{\omega} - J[R\dot{\boldsymbol{\omega}}_t + S(\boldsymbol{\omega})\boldsymbol{\omega}_e] + \boldsymbol{\tau} + \boldsymbol{d}_\tau \end{cases} \tag{7}$$

where $G(\boldsymbol{\sigma}_e) = (1/(4))[(1-\boldsymbol{\sigma}_e^T\boldsymbol{\sigma}_e)I_3 + 2S(\boldsymbol{\sigma}_e) + 2\boldsymbol{\sigma}_e\boldsymbol{\sigma}_e^T]$; $\boldsymbol{g}_e = S(\boldsymbol{\omega})\boldsymbol{v} - S(\boldsymbol{\omega}_e)(\boldsymbol{v}-\boldsymbol{v}_e) + \mu\boldsymbol{r}$; $R\dot{\boldsymbol{v}}_{p_t}$ can be calculated from (5), (2), (6), and $RS(\boldsymbol{a}) = S(R\boldsymbol{a})R$ for any $\boldsymbol{a} \in \mathbb{R}^3$ as

$$\begin{aligned} R\dot{\boldsymbol{v}}_{p_t} &= R[\dot{\boldsymbol{v}}_t + S(\dot{\boldsymbol{\omega}}_t)\boldsymbol{p}_t] \\ &= -RS(\boldsymbol{\omega}_t)\boldsymbol{v}_t - \mu_t R\boldsymbol{r}_t - RS(\boldsymbol{p}_t)\dot{\boldsymbol{\omega}}_t \\ &= -S(R\boldsymbol{\omega}_t)[R\boldsymbol{v}_{p_t} - RS(\boldsymbol{\omega}_t)\boldsymbol{p}_t] \\ &\quad + \mu_t R\boldsymbol{p}_t - \mu_t(\boldsymbol{r}-\boldsymbol{r}_e) - RS(\boldsymbol{p}_t)\dot{\boldsymbol{\omega}}_t \\ &= -S(\boldsymbol{\omega}-\boldsymbol{\omega}_e)[\boldsymbol{v} - \boldsymbol{v}_e - S(\boldsymbol{\omega}-\boldsymbol{\omega}_e)R\boldsymbol{p}_t] \\ &\quad + \mu_t R\boldsymbol{p}_t - \mu_t(\boldsymbol{r}-\boldsymbol{r}_e) - RS(\boldsymbol{p}_t)\dot{\boldsymbol{\omega}}_t \end{aligned} \tag{8}$$

and $\dot{\boldsymbol{\omega}}_t$ can be calculated from (2) as

$$\dot{\boldsymbol{\omega}}_t = -J_t^{-1}S(\boldsymbol{\omega}_t)J_t\boldsymbol{\omega}_t \tag{9}$$

Substituting (8) and (9) into (7) yields

$$\begin{cases} \dot{\boldsymbol{r}}_e = \boldsymbol{v}_e - S(\boldsymbol{\omega})\boldsymbol{r}_e \\ \dot{\boldsymbol{\sigma}}_e = G(\boldsymbol{\sigma}_e)\boldsymbol{\omega}_e \\ m\dot{\boldsymbol{v}}_e = -m\boldsymbol{g} + \boldsymbol{n}_1 + \boldsymbol{f} + \boldsymbol{d}_f \\ J\dot{\boldsymbol{\omega}}_e = -S(\boldsymbol{\omega})J\boldsymbol{\omega} - JS(\boldsymbol{\omega})\boldsymbol{\omega}_e + \boldsymbol{n}_2 + \boldsymbol{\tau} + \boldsymbol{d}_\tau \end{cases} \tag{10}$$

where $\boldsymbol{g} = S(\boldsymbol{\omega})\boldsymbol{v}_e + S^2(\boldsymbol{\omega}-\boldsymbol{\omega}_e)R\boldsymbol{p}_t + \mu\boldsymbol{r} + \mu_t R\boldsymbol{p}_t - \mu_t(\boldsymbol{r}-\boldsymbol{r}_e)$, $\boldsymbol{n}_1 = -mRS(\boldsymbol{p}_t)J_t^{-1}S(\boldsymbol{\omega}_t)J_t\boldsymbol{\omega}_t$, $\boldsymbol{n}_2 = JRJ_t^{-1}S(\boldsymbol{\omega}_t)J_t\boldsymbol{\omega}_t$.

With denoting the system states $\boldsymbol{e}_1 = [\boldsymbol{r}_e^T, \boldsymbol{\sigma}_e^T]^T$ and $\boldsymbol{e}_2 = [\boldsymbol{v}_e^T, \boldsymbol{\omega}_e^T]^T$, then the coupled relative dynamics (10) can be rewritten as

$$\begin{cases} \dot{\boldsymbol{e}}_1 = C_1\boldsymbol{e}_1 + C_2\boldsymbol{e}_2 \\ M\dot{\boldsymbol{e}}_2 = \boldsymbol{h} + \boldsymbol{n} + \boldsymbol{u} + \boldsymbol{d} \end{cases} \tag{11}$$

where $C_1 = \mathrm{diag}\{-S(\boldsymbol{\omega}), O_3\}$, $C_2 = \mathrm{diag}\{I_3, G(\boldsymbol{\sigma}_e)\}$, $M = \mathrm{diag}\{mI_3, J\}$, $\boldsymbol{n} = [\boldsymbol{n}_1^T, \boldsymbol{n}_2^T]^T$, $\boldsymbol{u} = [\boldsymbol{f}^T, \boldsymbol{\tau}^T]^T$, $\boldsymbol{d} = [\boldsymbol{d}_f^T, \boldsymbol{d}_\tau^T]^T$, and

$$\boldsymbol{h} = \begin{bmatrix} -m\boldsymbol{g} \\ -S(\boldsymbol{\omega})J\boldsymbol{\omega} - JS(\boldsymbol{\omega})\boldsymbol{\omega}_e \end{bmatrix}.$$

The terms C_1 and $\boldsymbol{n}$ indicate the kinematic couplings in spacecraft proximity maneuvers.

C. Control Objective

Consider that the chaser's control inputs $\boldsymbol{u} = [u_1, \ldots, u_6]^T$ are subject to the following constraints:

$$-u_{i_{\min}} \le u_i \le u_{i_{\max}}, \quad i = 1, \ldots, 6 \tag{12}$$

where $u_{i_{\min}}$ and $u_{i_{\max}}$ are the known lower and upper limits of input saturation constraints. Thus, the control input u_i is defined by

$$u_i = \begin{cases} u_{i_{\max}} & \text{if } u_{i_0} > u_{i_{\max}} \\ u_{i_0} & \text{if } -u_{i_{\min}} \le u_{i_0} \le u_{i_{\max}} \\ -u_{i_{\min}} & \text{if } u_{i_0} < -u_{i_{\min}} \end{cases} \tag{13}$$

where $\boldsymbol{u}_0 = [u_{1_0}, \ldots, u_{6_0}]^T$ is the control command to be designed in the presence of input saturation.

For system model (11), the following assumptions are employed in the subsequent development.

Assumption 1: Because of the fuel consumption, deployment of appendages, and the structural flexibility, the chaser's mass and inertial matrix are uncertain for the controller design. It is assumed that the chaser's mass and inertial matrix are,

respectively, denoted by $m = m_0 + m_\Delta$ and $J = J_0 + J_\Delta$, where m_0 and J_0 are estimations, and m_Δ and J_Δ are parametric uncertainties and they satisfy $|m_\Delta| \le \bar{m}_\Delta$ and $\|J_\Delta\| \le \bar{n}_\Delta$ with unknown positive constants $\bar{m}_\Delta$ and $\bar{n}_\Delta$. Meanwhile, the target's inertial matrix J_t is an unknown symmetric positive definite matrix for the chaser. Because of the short-time maneuvers in the proximity missions, external disturbance $\boldsymbol{d}$ is assumed to be bounded and its time derivative satisfies $\|\dot{\boldsymbol{d}}\| \le \delta_d$ with an unknown constant δ_d.

Assumption 2: The radius r_o of the target's circular orbit is assumed to be known for the chaser in advance, but the tumbling target's motion variables $\{\boldsymbol{r}_t, \boldsymbol{v}_t, \boldsymbol{\sigma}_t, \boldsymbol{\omega}_t\}$ are assumed to be unavailable directly for the chaser. The chaser's motion variables $\{\boldsymbol{r}, \boldsymbol{v}, \boldsymbol{\sigma}, \boldsymbol{\omega}\}$ are assumed to be directly measured or indirectly computed with the measurement devices mounted on the chaser's body [29], while the measurement accuracy and rate of these variables are assumed to be high enough so that the measurement errors can be omitted in the controller design.

Assumption 3: Due to the tumbling motion of the noncooperative target in the final proximity maneuvers, the relative motion variables are measured with measurement errors from many proximal sensors mounted on the chaser's body, such as light detection and ranging, laser dynamic range imager, and optical sensors combined with structured active light sources [7], [30], and then, the measurement quantities are expressed as

$$\begin{cases} \hat{\boldsymbol{e}}_1 = \boldsymbol{e}_1 + \boldsymbol{\delta}_{e1} \\ \hat{\boldsymbol{e}}_2 = \boldsymbol{e}_1 + \boldsymbol{\delta}_{e2} \end{cases} \tag{14}$$

where $\hat{\boldsymbol{e}}_1 = [\hat{\boldsymbol{r}}_e^T, \hat{\boldsymbol{\sigma}}_e^T]^T$, $\hat{\boldsymbol{e}}_2 = [\hat{\boldsymbol{v}}_e^T, \hat{\boldsymbol{\omega}}_e^T]^T$; $\boldsymbol{\delta}_{e1} = [\boldsymbol{\delta}_{re}^T, \boldsymbol{\delta}_{\sigma e}^T]^T$ and $\boldsymbol{\delta}_{e2} = [\boldsymbol{\delta}_{ve}^T, \boldsymbol{\delta}_{\omega e}^T]^T$ are the measurement errors. It is assumed that [31], [32] $\hat{\boldsymbol{e}}_i(t)(i = 1, 2)$ is continuous, $\boldsymbol{\delta}_{ei}(t)$ is differentiable, and $\dot{\boldsymbol{\delta}}_{ei}(t)$ is bounded for all $t \ge 0$. Moreover, there exists positive scalars $\bar{\delta}_{ei}$ and $\bar{\dot{\delta}}_{ei}$, such that $\|\boldsymbol{\delta}_{ei}(t)\| \le \bar{\delta}_{ei}$ and $\|\dot{\boldsymbol{\delta}}_{ei}(t)\| \le \bar{\dot{\delta}}_{ei}$.

Based on the model (11) and Assumptions 1–3, the problem of positioning the chaser at a desired position $\boldsymbol{p}_t$ and rotating the chaser to coincide with the target's attitude can be formulated as a regulation problem. The control objective for model (11) is to design robust saturated control inputs, such that the controlled spacecraft proximity system with modeling uncertainties is capable to guarantee $\lim_{t\to\infty} \|\hat{\boldsymbol{e}}_1(t)\| \le \epsilon$, where $\epsilon > 0$ represents the required bound of the final relative motion errors between two spacecraft.

III. Main Results

Define a vector

$$\hat{\boldsymbol{s}} = \hat{\boldsymbol{e}}_2 + \Lambda \hat{\boldsymbol{e}}_1 \tag{15}$$

where $\Lambda = \mathrm{diag}\{\Lambda_1, \Lambda_2\}$, and $\Lambda_i \in \mathbb{R}^{3\times 3}(i = 1, 2)$ are positive definite diagonal gain matrices. Then, the measurement model for (11) can be written as

$$\begin{cases} \dot{\hat{\boldsymbol{e}}}_1 = C_1 \hat{\boldsymbol{e}}_1 + \hat{C}_2 \hat{\boldsymbol{e}}_2 + \boldsymbol{\delta}_a \\ M_0 \dot{\hat{\boldsymbol{s}}} = \hat{\boldsymbol{h}}_s + \boldsymbol{u} + \boldsymbol{w} \end{cases} \tag{16}$$

with the system lumped disturbance

$$\boldsymbol{w} = \boldsymbol{d} + \boldsymbol{n} + \boldsymbol{\xi} \tag{17}$$

where $\hat{C}_2 = \mathrm{diag}\{I_3, G(\hat{\boldsymbol{\sigma}}_e)\}$, $\boldsymbol{\delta}_a = \dot{\boldsymbol{\delta}}_{e1} - C_1\boldsymbol{\delta}_{e1} - \hat{C}_2\boldsymbol{\delta}_{e2} - \Delta_{C2}(\hat{\boldsymbol{e}}_2 - \boldsymbol{\delta}_{e2})$, $\Delta_{C2} = \mathrm{diag}\{I_3, G(\boldsymbol{\delta}_{\sigma e})\}$, $\hat{\boldsymbol{h}}_s = \hat{\boldsymbol{h}}_0 + M_0\Lambda C_1\hat{\boldsymbol{e}}_1 + M_0\Lambda\hat{C}_2\hat{\boldsymbol{e}}_2$, $\boldsymbol{\xi} = \boldsymbol{\delta}_{h0} + \boldsymbol{h}_\Delta + M_0\Lambda\boldsymbol{\delta}_a + M_0\Lambda\dot{\boldsymbol{\delta}}_{e1} + M_\Delta\Lambda(\dot{\hat{\boldsymbol{e}}}_1 - \dot{\boldsymbol{\delta}}_{e1}) - M_\Delta\dot{\hat{\boldsymbol{s}}}$, $M_0 = \mathrm{diag}\{m_0 I_3, J_0\}$, $M_\Delta = \mathrm{diag}\{m_\Delta I_3, J_\Delta\}$

$$\hat{\boldsymbol{h}}_0 = \begin{bmatrix} -m_0\hat{\boldsymbol{g}} \\ -S(\boldsymbol{\omega})J_0\boldsymbol{\omega} - J_0 S(\boldsymbol{\omega})\hat{\boldsymbol{\omega}}_e \end{bmatrix}$$

$$\boldsymbol{\delta}_{h0} = \begin{bmatrix} -m_0\boldsymbol{\delta}_g \\ -S(\boldsymbol{\omega})J_0\boldsymbol{\omega} - J_0 S(\boldsymbol{\omega})\boldsymbol{\delta}_{\omega e} \end{bmatrix}$$

$$\boldsymbol{h}_\Delta = \begin{bmatrix} -m_\Delta(\hat{\boldsymbol{g}} + \boldsymbol{\delta}_g) \\ -S(\boldsymbol{\omega})J_\Delta\boldsymbol{\omega} - J_\Delta S(\boldsymbol{\omega})(\hat{\boldsymbol{\omega}}_e + \boldsymbol{\delta}_{\omega e}) \end{bmatrix}$$

$\hat{\boldsymbol{g}} = S(\boldsymbol{\omega})\hat{\boldsymbol{v}}_e + S^2(\boldsymbol{\omega} - \hat{\boldsymbol{\omega}}_e)\hat{R}\boldsymbol{p}_t + \mu\boldsymbol{r} + \mu_t\hat{R}\boldsymbol{p}_t - \mu_t(\boldsymbol{r} - \hat{\boldsymbol{r}}_e)$, $\boldsymbol{\delta}_g = S(\boldsymbol{\omega})\boldsymbol{\delta}_{ve} + S^2(\boldsymbol{\omega})R_\delta\boldsymbol{p}_t + S^2(\hat{\boldsymbol{\omega}}_e)R_\delta\boldsymbol{p}_t + S^2(\boldsymbol{\delta}_{\omega e})(\hat{R} - R_\delta)\boldsymbol{p}_t + \mu_t R_\delta\boldsymbol{p}_t + \mu_t\boldsymbol{\delta}_{re}$, $\hat{R} = R(\hat{\boldsymbol{\sigma}}_e)$, $R_\delta = R(\boldsymbol{\delta}_{\sigma e})$.

A. Disturbance Observer Design

For the close proximity maneuver, precisely modeling its dynamics or directly measuring the disturbances acting on it is very difficult. However, the disturbance observer technique provides an alternative approach. Applying the exponential convergent observer for a general nonlinear system from [13], we construct the nonlinear disturbance observer for the lumped disturbance vector $\boldsymbol{w}$ in (17) as follows:

$$\begin{cases} \hat{\boldsymbol{w}} = \boldsymbol{z} + \Gamma M_0\hat{\boldsymbol{s}} \\ \dot{\boldsymbol{z}} = -\Gamma\boldsymbol{z} - \Gamma(\hat{\boldsymbol{h}}_s + \boldsymbol{u} + \Gamma M_0\hat{\boldsymbol{s}}) \end{cases} \tag{18}$$

where $\hat{\boldsymbol{w}}$ is the disturbance observation, $\boldsymbol{z}$ is the state vector of the disturbance observer, and $\Gamma \in \mathbb{R}^{6\times 6}$ is a positive definite diagonal gain matrix for observer.

Define the observation error $\tilde{\boldsymbol{w}}$ of the lumped disturbance $\boldsymbol{w}$ as $\tilde{\boldsymbol{w}} = \boldsymbol{w} - \hat{\boldsymbol{w}}$. From (16) and (18), we have

$$\begin{aligned} \dot{\tilde{\boldsymbol{w}}} &= \dot{\boldsymbol{z}} + \Gamma M_0\dot{\hat{\boldsymbol{s}}} \\ &= -\Gamma\boldsymbol{z} - \Gamma(\hat{\boldsymbol{h}}_s + \boldsymbol{u} + \Gamma M_0\hat{\boldsymbol{s}}) + \Gamma(\hat{\boldsymbol{h}}_s + \boldsymbol{u} + \boldsymbol{w}) \\ &= \Gamma[\boldsymbol{w} - (\boldsymbol{z} + \Gamma M_0\hat{\boldsymbol{s}})] \\ &= \Gamma(\boldsymbol{w} - \hat{\boldsymbol{w}}). \end{aligned} \tag{19}$$

Then, the time derivative of $\tilde{\boldsymbol{w}}$ is

$$\dot{\tilde{\boldsymbol{w}}} = \dot{\boldsymbol{w}} - \Gamma(\boldsymbol{w} - \hat{\boldsymbol{w}}) = \dot{\boldsymbol{w}} - \Gamma\tilde{\boldsymbol{w}}. \tag{20}$$

Therefore, we have the following theorem.

Theorem 1: If the lumped disturbance vector $\boldsymbol{w}$ in (17) satisfies $\|\dot{\boldsymbol{w}}\| \le \beta$ with a positive scalar β, then the disturbance observer (18) guarantees that disturbance observation error $\tilde{\boldsymbol{w}}$ is always bounded.

Proof: Choose a Lyapunov function candidate $V_w = (1/(2))\tilde{\boldsymbol{w}}^T\tilde{\boldsymbol{w}} \ge 0$. The time derivative of V_w along the solution of (20) is $\dot{V}_w = -\tilde{\boldsymbol{w}}^T\Gamma\tilde{\boldsymbol{w}} + \tilde{\boldsymbol{w}}^T\dot{\boldsymbol{w}} \le -\lambda_m(\Gamma)\tilde{\boldsymbol{w}}^T\tilde{\boldsymbol{w}} + \tilde{\boldsymbol{w}}^T\dot{\boldsymbol{w}}$, where $\lambda_m(\Gamma)$ is the minimum eigenvalue of matrix Γ. Then, by applying Young inequality [13] and $\|\dot{\boldsymbol{w}}\| \le \beta$, we obtain $\dot{V}_w \le -\lambda_m(\Gamma)V_w + (\beta^2/(2\lambda_m(\Gamma)))$. Then, we have $V_w(t) \le (\beta^2/(2\lambda_m^2(\Gamma))) + [V_w(0) - (\beta^2/(2\lambda_m^2(\Gamma)))]e^{-\lambda_m(\Gamma)t}$.

From the definition of V_w, we also have $\lim_{t\to\infty}\|\tilde{\boldsymbol{w}}(t)\| \le (\beta/(\lambda_m(\Gamma)))$. Thus, disturbance observation error $\tilde{\boldsymbol{w}}$ is always bounded, if the lumped disturbance vector $\boldsymbol{w}$ satisfies $\|\dot{\boldsymbol{w}}\| \le \beta$ with a positive constant β. ■

B. Robust Saturated Controller Design

Based on the observation of lumped disturbance, control input command for system model (16) can be designed as follows:

$$\boldsymbol{u}_0 = -\hat{C}_2^T\hat{\boldsymbol{e}}_1 - K_1\hat{\boldsymbol{s}} + K_2\boldsymbol{\zeta} - \hat{\boldsymbol{h}}_s - \hat{\boldsymbol{w}} \tag{21}$$

and $\boldsymbol{\zeta}$ is the output of the following saturation compensator:

$$\dot{\boldsymbol{\zeta}} = -K_3\boldsymbol{\zeta} + \boldsymbol{u}_\Delta \tag{22}$$

where $K_i (i = 1, 2, 3)$ are 6×6 positive definite diagonal gain matrices, and $\boldsymbol{u}_\Delta = \boldsymbol{u} - \boldsymbol{u}_0$.

Remark 1: The linear first-order system (22) is designed as the classical antiwindup compensator, where the term $\boldsymbol{\zeta}$ is the state of the compensator and it is used in controller to handle the adverse effect of input saturation. The main characteristic of this scheme is that the differences between the actual actuator output and the unconstraint controller output, which correspond to the nonlinear term $\boldsymbol{u}_\Delta = \boldsymbol{u} - \boldsymbol{u}_0$ is fed back through the gain K_2 in (21) in order to affect the evolution of controllers and system states.

Substituting control command (21) into (16) and combining with the proposed observer (18) give rise to the closed-loop system of spacecraft proximity maneuvers as

$$\begin{cases}\dot{\hat{\boldsymbol{e}}}_1 = C_1\hat{\boldsymbol{e}}_1 + \hat{C}_2\hat{\boldsymbol{e}}_2 + \boldsymbol{\delta}_a\\ M_0\dot{\hat{\boldsymbol{s}}} = -\hat{C}_2^T\hat{\boldsymbol{e}}_1 - K_1\hat{\boldsymbol{s}} + K_2\boldsymbol{\zeta} + \boldsymbol{u}_\Delta + \tilde{\boldsymbol{w}}\end{cases} \tag{23}$$

Therefore, we have the following theorem.

Theorem 2: Under Assumptions 1–3, for the spacecraft proximity maneuvers model (11) with parametric uncertainties, kinematic couplings, and unknown disturbances, the saturated controller described by (21) together with disturbance observer (18) and saturation compensator (22) guarantees that all signals of the closed-loop system (23) converge to sufficiently small neighborhood of the origin by appropriately adjusting the gain matrices $K_i (i = 1, 2, 3)$, Λ, and Γ according to the conditions (27) and (28).

Proof: Choose a Lyapunov function candidate

$$V = \frac{1}{2}\hat{\boldsymbol{e}}_1^T\hat{\boldsymbol{e}}_1 + \frac{1}{2}\hat{\boldsymbol{s}}^T M_0\hat{\boldsymbol{s}} + \frac{1}{2}\boldsymbol{\zeta}^T\boldsymbol{\zeta} + V_w \ge 0 \tag{24}$$

The time derivative of V along the trajectory of the closed-loop system (23) is

$$\begin{aligned}\dot{V} &= \hat{\boldsymbol{e}}_1^T(C_1\hat{\boldsymbol{e}}_1 + \hat{C}_2\hat{\boldsymbol{e}}_2 + \boldsymbol{\delta}_a) + \hat{\boldsymbol{s}}^T\big(-\hat{C}_2^T\hat{\boldsymbol{e}}_1 - K_1\hat{\boldsymbol{s}} + K_2\boldsymbol{\zeta}\\ &\qquad + \boldsymbol{u}_\Delta + \tilde{\boldsymbol{w}}\big)\\ &\quad - \boldsymbol{\zeta}^T K_3\boldsymbol{\zeta} + \boldsymbol{\zeta}^T\boldsymbol{u}_\Delta + \tilde{\boldsymbol{w}}^T(\dot{\boldsymbol{w}} - \Gamma\tilde{\boldsymbol{w}})\end{aligned} \tag{25}$$

Since $\hat{\boldsymbol{e}}_1^T C_1\hat{\boldsymbol{e}}_1 = 0$, $\hat{\boldsymbol{e}}_2 = \hat{\boldsymbol{s}} - \Lambda\hat{\boldsymbol{e}}_1$, and $\hat{\boldsymbol{\sigma}}_e^T G(\hat{\boldsymbol{\sigma}}_e) = (1/(4))(1+\hat{\boldsymbol{\sigma}}_e^T\hat{\boldsymbol{\sigma}}_e)\hat{\boldsymbol{\sigma}}_e^T$, then by applying Young inequality [13], we derive

$$\begin{aligned}\dot{V} &= -\hat{\boldsymbol{e}}_1^T\Lambda_c\hat{\boldsymbol{e}}_1 + \hat{\boldsymbol{e}}_1^T\boldsymbol{\delta}_a - \hat{\boldsymbol{s}}^T K_1\hat{\boldsymbol{s}} + \hat{\boldsymbol{s}}^T K_2\boldsymbol{\zeta} + \hat{\boldsymbol{s}}^T\boldsymbol{u}_\Delta + \hat{\boldsymbol{s}}^T\tilde{\boldsymbol{w}}\\ &\quad - \boldsymbol{\zeta}^T K_3\boldsymbol{\zeta} + \boldsymbol{\zeta}^T\boldsymbol{u}_\Delta - \tilde{\boldsymbol{w}}^T\Gamma\tilde{\boldsymbol{w}} + \tilde{\boldsymbol{w}}^T\dot{\boldsymbol{w}}\\ &\le -\frac{1}{8}\lambda_m(\Lambda)\|\hat{\boldsymbol{e}}_1\|^2 + \frac{2\|\boldsymbol{\delta}_a\|^2}{\lambda_m(\Lambda)} - \frac{1}{4}\lambda_m(K_1)\|\hat{\boldsymbol{s}}\|^2\\ &\quad - \left[\frac{1}{2}\lambda_m(K_3) - \frac{\bar{\lambda}^2(K_2)}{\lambda_m(K_1)}\right]\|\boldsymbol{\zeta}\|^2\\ &\quad - \left[\frac{1}{2}\lambda_m(\Gamma) - \frac{1}{\lambda_m(K_1)}\right]\|\tilde{\boldsymbol{w}}\|^2 + \frac{1}{2\lambda_m(\Gamma)}\|\dot{\boldsymbol{w}}\|^2\\ &\quad + \left[\frac{1}{\lambda_m(K_1)} + \frac{1}{2\lambda_m(K_3)}\right]\|\boldsymbol{u}_\Delta\|^2\end{aligned} \tag{26}$$

where $\Lambda_c = \mathrm{diag}\{\Lambda_1, (1/(4))(1+\hat{\boldsymbol{\sigma}}_e^T\hat{\boldsymbol{\sigma}}_e)\Lambda_2\}$, $\bar{\lambda}(K_2)$ is the maximum eigenvalue of matrix K_2, and $\lambda_m(\Lambda)$ and $\lambda_m(K_i)$ are minimum eigenvalues of matrices Λ and $K_i (i = 1, 2, 3)$, respectively. Furthermore, if

$$\frac{1}{2}\lambda_m(K_3) - \frac{\bar{\lambda}^2(K_2)}{\lambda_m(K_1)} > 0, \quad \frac{1}{2}\lambda_m(\Gamma) - \frac{1}{\lambda_m(K_1)} > 0 \tag{27}$$

then, $\dot{V} \le -a\|\boldsymbol{x}\|^2 + b$, where $\boldsymbol{x} = [\hat{\boldsymbol{e}}_1^T, \hat{\boldsymbol{s}}^T, \boldsymbol{\zeta}^T, \tilde{\boldsymbol{w}}^T]^T$; $a = \min\{(1/(8))\lambda_m(\Lambda), (1/(4))\lambda_m(K_1), (1/(2))\lambda_m(K_3) - (\bar{\lambda}^2(K_2)/(\lambda_m(K_1))), (1/(2))\lambda_m(\Gamma) - (1/(\lambda_m(K_1)))\}$, $b = (\|\dot{\boldsymbol{w}}\|^2/(2\lambda_m(\Gamma))) + [(1/(\lambda_m(K_1))) + (1/(2\lambda_m(K_3)))]\|\boldsymbol{u}_\Delta\|^2 + (2\|\boldsymbol{\delta}_a\|^2/(\lambda_m(\Lambda)))$.

Recalling model (2) gives rise to $\|\boldsymbol{\omega}_t\| \le ((E(0)/(\lambda_m(J_t))))^{1/2} \triangleq \alpha_1$, where $E(0) = \mu_t m_t\|\boldsymbol{r}_t(0)\|^2 + m_t\|\boldsymbol{v}_t(0)\|^2 + \boldsymbol{\omega}_t^T(0)J_t\boldsymbol{\omega}_t(0)$, and $\lambda_m(J_t)$ is the minimum eigenvalue of the matrix J_t. From $\dot{R} = -S(\boldsymbol{\omega}_e)R$, the expression of $\dot{\boldsymbol{\omega}}_t$ in (9), and the definition of $\boldsymbol{n}$ in (11), we know $\dot{\boldsymbol{n}}_1 = mS(\boldsymbol{\omega}_e)RS(\boldsymbol{p}_t)J_t^{-1}S(\boldsymbol{\omega}_t)J_t\boldsymbol{\omega}_t - mRS(\boldsymbol{p}_t)J_t^{-1}S(J_t\boldsymbol{\omega}_t)J_t^{-1}S(\boldsymbol{\omega}_t)J_t\boldsymbol{\omega}_t + mRS(\boldsymbol{p}_t)J_t^{-1}S(\boldsymbol{\omega}_t)J_tS^2(\boldsymbol{\omega}_t)J_t\boldsymbol{\omega}_t$ and $\dot{\boldsymbol{n}}_2 = -JS(\boldsymbol{\omega}_e)RJ_t^{-1}S(\boldsymbol{\omega}_t)J_t\boldsymbol{\omega}_t + JRJ_t^{-1}S(J_t\boldsymbol{\omega}_t)J_t^{-1}S(\boldsymbol{\omega}_t)J_t\boldsymbol{\omega}_t - JRJ_t^{-1}S(\boldsymbol{\omega}_t)J_tS^2(\boldsymbol{\omega}_t)J_t\boldsymbol{\omega}_t$ then from $\|R\| = 1$ and $\|S(\boldsymbol{a})\| = \|\boldsymbol{a}\|$ for any $\boldsymbol{a} \in \mathbb{R}^3$, we can conclude $\|\dot{\boldsymbol{n}}_1\| \le m\|\boldsymbol{p}_t\|\|\omega_e\|\|J_t^{-1}\|\|J_t\|\alpha_1^2 + m\|\boldsymbol{p}_t\|\|J_t^{-1}\|^2\|J_t\|^2\alpha_1^3 + m\|\boldsymbol{p}_t\|\|J_t^{-1}\|\|J_t\|^2\alpha_1^4$ and $\|\dot{\boldsymbol{n}}_2\| \le \|J\|\|\omega_e\|\|J_t^{-1}\|\|J_t\|\alpha_1^2 + \|J\|\|J_t^{-1}\|^2\|J_t\|^2\alpha_1^3 + \|J\|\|J_t^{-1}\|\|J_t\|^2\alpha_1^4$, thus $\|\dot{\boldsymbol{n}}\| \le \|\dot{\boldsymbol{n}}_1\| + \|\dot{\boldsymbol{n}}_2\| \le \kappa_1\|\boldsymbol{\omega}_e\| + \kappa_2$, where $\kappa_1 = (m\|\boldsymbol{p}_t\| + \|J\|)\|J_t^{-1}\|\|J_t\|\alpha_1^2$ and $\kappa_2 = (m\|\boldsymbol{p}_t\| + \|J\|)[\|J_t^{-1}\|^2\|J_t\|^2\alpha_1^3 + \|J_t^{-1}\|\|J_t\|^2\alpha_1^4]$.

Under the mild assumptions that $\boldsymbol{\delta}_a(t)$ is a continuously bounded function and $\boldsymbol{\xi}(t)$ is a continuously slower varying function compared with the dynamics of disturbance observer, we have $\|\boldsymbol{\delta}_a(t)\| \le \delta_0$ and $\|\dot{\boldsymbol{\xi}}(t)\| \le \eta_0$ with unknown scalars δ_0 and η_0 based on existing works in [33][34], then according to $\|\hat{\boldsymbol{\omega}}_e\| \le \|\hat{\boldsymbol{e}}_2\| \le (1 + \|\Lambda\|)\|\boldsymbol{x}_s\|$ with $\boldsymbol{x}_s = [\hat{\boldsymbol{e}}_1^T, \hat{\boldsymbol{s}}^T]^T$, and $\|\dot{\boldsymbol{d}}\| \le \delta_d$ in Assumption 1, we have $\|\dot{\boldsymbol{w}}\| \le \|\dot{\boldsymbol{d}}\| + \|\dot{\boldsymbol{n}}\| + \|\dot{\boldsymbol{\xi}}\| \le \eta_1\|\boldsymbol{x}_s\| + \eta_2$, where $\eta_1 = \kappa_1(1 + \|\Lambda\|)$ and $\eta_2 = \delta_d + \kappa_1\bar{\delta}_{e2} + \kappa_2 + \eta_0$. Then, from $\|\boldsymbol{x}_s\| \le \|\boldsymbol{x}\|$, we also have $\|\dot{\boldsymbol{w}}\|^2 \le (\eta_1\|\boldsymbol{x}\| + \eta_2)^2 = \eta_1^2\|\boldsymbol{x}\|^2 + 2\eta_1\eta_2\|\boldsymbol{x}\| + \eta_2^2$. Thus, if $2a\lambda_m(\Gamma) > \eta_1^2$, namely

$$\frac{2a\lambda_m(\Gamma)}{(1 + \|\Lambda\|)^2} > \kappa_1^2 \tag{28}$$

then, from $\dot{V} \le -a\|\boldsymbol{x}\|^2 + b$, we have

$$\begin{aligned}\dot{V} &\le -\left[a - \frac{\eta_1^2}{2\lambda_m(\Gamma)}\right]\|\boldsymbol{x}\|^2 + \frac{\eta_1\eta_2\|\boldsymbol{x}\|}{\lambda_m(\Gamma)} + \frac{\eta_2^2}{2\lambda_m(\Gamma)} \\ &\quad + \left[\frac{1}{\lambda_m(K_1)} + \frac{1}{2\lambda_m(K_3)}\right]\|\boldsymbol{u}_\Delta\|^2 + \frac{2\delta_0^2}{\lambda_m(\Lambda)} \\ &= -\bar{a}\|\boldsymbol{x}\|^2 - \bar{a}\left[\|\boldsymbol{x}\| - \frac{2\eta_1\eta_2}{2\lambda_m(\Gamma)a - \eta_1^2}\right]^2 \\ &\quad + \frac{4\eta_1^2\eta_2^2}{[2a\lambda_m(\Gamma) - \eta_1^2]^2} + \frac{\eta_2^2}{2\lambda_m(\Gamma)} \\ &\quad + \left[\frac{1}{\lambda_m(K_1)} + \frac{1}{2\lambda_m(K_3)}\right]\|\boldsymbol{u}_\Delta\|^2 + \frac{2\delta_0^2}{\lambda_m(\Lambda)} \\ &\le -\bar{a}\|\boldsymbol{x}\|^2 + \bar{b} \end{aligned} \tag{29}$$

where $\bar{a} = (1/(2))[a - (\eta_1^2/(2\lambda_m(\Gamma)))]$ and $\bar{b} = (4\eta_1^2\eta_2^2/([2a\lambda_m(\Gamma) - \eta_1^2]^2)) + (\eta_2^2/(2\lambda_m(\Gamma))) + [(1/(\lambda_m(K_1))) + (1/(2\lambda_m(K_3)))]\|\boldsymbol{u}_\Delta\|^2 + (2\delta_0^2/(\lambda_m(\Lambda)))$.

From the definition of V in (24), we have $\bar{c}\|\boldsymbol{x}\|^2 \le V \le \bar{d}\|\boldsymbol{x}\|^2$, where $\bar{c} = (1/(2))\min\{1, \lambda_m(M)\}$, $\bar{d} = (1/(2))\max\{1, \lambda_M(M)\}$; $\lambda_m(M)$ and $\lambda_M(M)$ are minimum and maximum eigenvalues of matrix M, respectively. Then, (29) can be rewritten as $\dot{V} \le -(\bar{a}/(\bar{d}))V + \bar{b}$. Then, we have $V(t) \le (\bar{d}\bar{b}/(\bar{a})) + [V(0) - (\bar{d}\bar{b}/(\bar{a}))]e^{-(\bar{a}/(\bar{d}))t}$ and $\lim_{t\to\infty}\|\hat{\boldsymbol{e}}_1(t)\| \le \lim_{t\to\infty}\|\boldsymbol{x}(t)\| \le ((\bar{d}\bar{b}/(\bar{a}\bar{c})))^{1/2} < \epsilon$. Hence, $\hat{\boldsymbol{e}}_1(t)$ converges to the desired ϵ-neighborhood of the origin as $t \to \infty$ by adjusting gains of controller and observer, and larger gain matrices K_1, K_3, Λ, Γ, and smaller K_2 give rise to smaller $\|\hat{\boldsymbol{e}}_1(\infty)\|$; control objective can be achieved. ■

Remark 2: The ultimate bound of $\|\hat{\boldsymbol{e}}_1(t)\|$ mainly depends on $\bar{a}$ and $\bar{b}$, while larger $\bar{a}$ and smaller $\bar{b}$ result in smaller $\|\hat{\boldsymbol{e}}_1(\infty)\|$. Since the saturation compensator (22) is bounded input bounded output linear system and the state of the saturation compensator $\boldsymbol{\zeta}$ is uniformly ultimately bounded, then the term $\boldsymbol{u}_\Delta$ involved in $\bar{d}$ is also bounded. Because κ_1, κ_2, δ, and η_0 are bounded, from the definition of η_1, $\bar{a}$, and $\bar{b}$ in (29), we know larger K_1, K_3, Λ, Γ, and smaller K_2 lead to larger a and smaller $\bar{b}$. Moreover, since Λ is involved in η_1, thus $\lambda_m(\Gamma) > \lambda_M(\Lambda)$ should be satisfied at least, so that $(2a\lambda_m(\Gamma)/((1 + \|\Lambda\|)^2)) > \kappa_1^2$, $\bar{b}$ is small enough and $\bar{a}$ is large enough. Thus, $\|\hat{\boldsymbol{e}}_1(\infty)\| < \epsilon$ can be achieved. Moreover, if choosing smaller K_1 and larger Γ, then the observer dynamics is faster than the lumped disturbance, so that lumped disturbance related to system states can be reasonably estimated [17].

IV. Simulation Example

In this section, the simulation describes an example of the autonomous R-bar proximity mission in orbit, in which the target spacecraft has a lower dynamic operating condition so that the docking can be safely carried out and supported. After the relative position and the attitude of the spacecraft have been precisely controlled, the docking ports of the two spacecraft will be well aligned without relative motions. Simulation results demonstrate the performance of the developed controller and observer.

Suppose the target moves in a circular orbit, and chaser's initial position, velocity, attitude, and angular velocity are $\boldsymbol{r}(0) = [1, 1, 1]^T \times 7.078 \times 10^8$(m), $\boldsymbol{v}(0) = [2, 3, -2]^T \times 10^3$(m/s), $\boldsymbol{\sigma}(0) = [0, 0, 0]^T$, and $\boldsymbol{\omega}(0) = [0, 0, 0]^T$(rad/s), respectively. Initially, measurement quantities of relative position, relative velocity, relative attitude, and relative angular velocity between two spacecraft are $\hat{\boldsymbol{r}}_e(0) = [50/\sqrt{2}, 0, -50/\sqrt{2}]^T$(m), $\hat{\boldsymbol{v}}_e(0) = [0.5, -0.5, 0.5]^T$(m/s), $\hat{\boldsymbol{\sigma}}_e(0) = [0.5, -0.6, 0.7]^T$, and $\hat{\boldsymbol{\omega}}_e(0) = [0.02, -0.02, 0.02]^T$(rad/s), respectively. The perfect measurements of relative position and relative attitude are corrupted by truncated Gaussian white noises of variances 0.001(m/s$^{1/2}$) and $100\ \mu$(rad/s$^{1/2}$) to model the measurement errors [7]. In case of any relative navigation sensors, a truncated Gaussian white noise depicts the nominal geometric state estimation error; note the worst case measurement errors are physically bounded by the sensor field of view. For simulation purpose, the state information is assumed to be available at a frequency of 100(Hz), which is generally the case for many relative navigation sensors. The desired position of the chaser in frame $\mathcal{F}_t$ is $\boldsymbol{p}_t = [0, 5, 0]^T$(m). The known lower and upper limits of input saturation constraints are $\boldsymbol{u}_{\min} = \boldsymbol{u}_{\max} = [20, 20, 20, 10, 10, 10]^T$, respectively. The desired ultimate bound of the relative motion errors is set as $\epsilon = 0.05$. The controller and observer gains are selected by trial and error as $K_1 = \text{diag}\{20I_3, 200I_3\}$, $K_2 = I_6$, $K_3 = 0.2I_6$, $\Lambda = \text{diag}\{0.02I_3, 0.15I_3\}$, and $\Gamma = 0.3I_6$. The estimation of chaser's mass and inertial matrix is $m_0 = 0.8m$(kg) and $J_0 = 0.8J$(kgm^2), where m and J are shown as follows.

In the simulation, the parameters of the chaser, the target, and external disturbances are selected as [25]

$$\begin{aligned} m &= 58.2\ \text{(kg)} \\ J &= \begin{bmatrix} 598.3 & -22.5 & -51.5 \\ -22.5 & 424.4 & -27 \\ -51.5 & -27 & 263.6 \end{bmatrix} (\text{kgm}^2) \\ J_t &= \begin{bmatrix} 3336 & -135.4 & -154.2 \\ -135.4 & 3185 & -148.5 \\ -154.2 & -148.5 & 2424 \end{bmatrix} (\text{kgm}^2) \\ \boldsymbol{d}_\tau &= \begin{bmatrix} 0.06 - 0.04\sin(\omega_o t) + 0.05\cos(\omega_o t) \\ 0.07 + 0.05\sin(\omega_o t) - 0.04\cos(\omega_o t) \\ 0.04 - 0.03\sin(\omega_o t) + 0.03\cos(\omega_o t) \end{bmatrix} \\ &\quad + \bar{\boldsymbol{\zeta}}_1(\text{Nm}) \\ \boldsymbol{d}_f &= \begin{bmatrix} 0.3 - 0.2\sin(\omega_o t) - 0.4\cos(\omega_o t) \\ 0.3 - 0.3\sin(\omega_o t) + 0.2\cos(\omega_o t) \\ 0.2 + 0.4\sin(\omega_o t) + 0.2\cos(\omega_o t) \end{bmatrix} \\ &\quad + \bar{\boldsymbol{\zeta}}_2(\text{N}). \end{aligned}$$

where $\bar{\boldsymbol{\zeta}}_1 = 0.25 \times \text{randn}(3, 1)$ and $\bar{\boldsymbol{\zeta}}_2 = 0.5 \times \text{randn}(3, 1)$ are the additive random noises. It is noted that the disturbance force $\boldsymbol{d}_f$ and torque $\boldsymbol{d}_\tau$ exerted on the chaser can be viewed as a function of the chaser's orbital angular velocity $\omega_o = (\mu_g/\|\boldsymbol{r}\|^3)^{1/2}$, and the gravitational constant of the earth is $\mu_g = 3.986 \times 10^{14}$(m^3/s^2). Except for typical periodic disturbance [4] exerted on the chaser, the random noises from the space environment is another disturbance source for the spacecraft, and thus, $\boldsymbol{\zeta}_1$ and $\boldsymbol{\zeta}_2$ are added in the disturbance

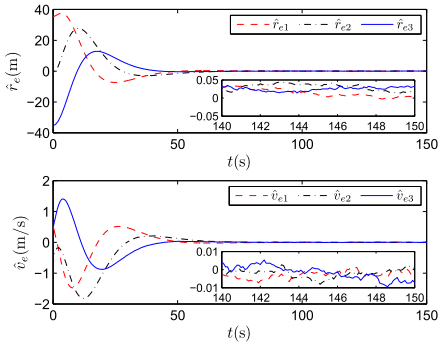

Fig. 2. Response of relative position motion under (21).

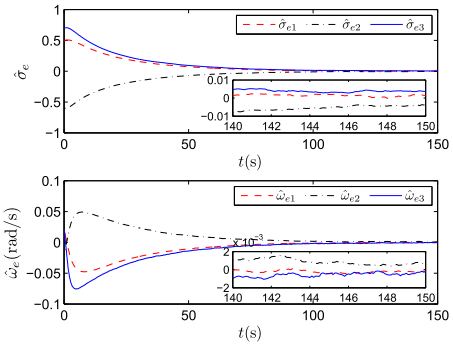

Fig. 3. Response of relative attitude motion under (21).

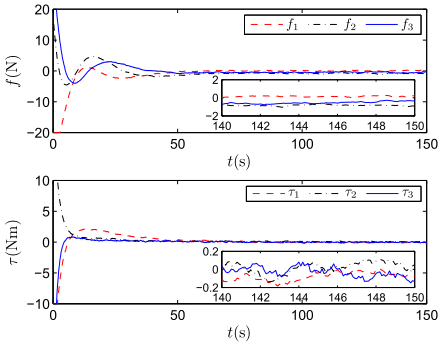

Fig. 4. Response of control forces and control torques under (21).

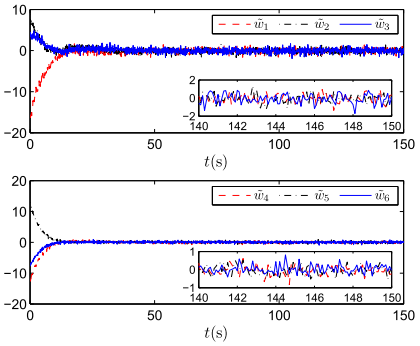

Fig. 5. Response of lumped disturbance observation errors under (21).

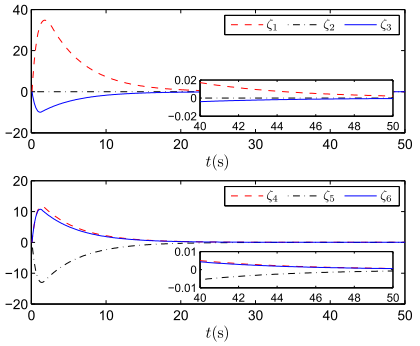

Fig. 6. Response of saturation compensator states under (21).

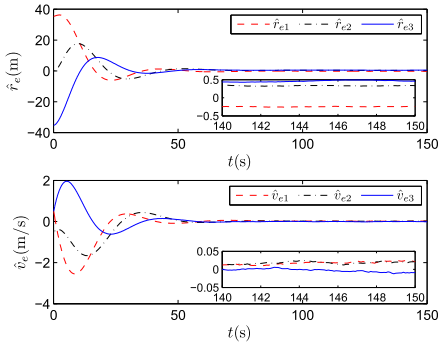

Fig. 7. Response of relative position motion without (18) and (22).

torques $\boldsymbol{d}_\tau$ and forces $\boldsymbol{d}_f$, respectively, to obtain controller responses in nearly practical environments [8].

Fig. 2 shows the response of relative position and relative velocity. The relative position control objective is to drive the chaser to a position of $\boldsymbol{p}_t = [0, 5, 0]^T$ (m) in $\mathcal{F}_t$. As can be seen, the desired position is reached in about 80 (s). The relative velocity in $\mathcal{F}_c$ goes to zero so that there is no relative translational motion. The relative attitude motion is shown in Fig. 3 including the relative attitude and relative angular velocities that are represented in $\mathcal{F}_c$. The relative attitude converging to zero indicates that the attitude of the chaser is synchronized with the attitude of the target. The attitude synchronization is achieved in about 120 (s). These results demonstrate a good attitude tracking performance. The control forces and control torques presented in Fig. 4 show that the initial control efforts are large in order to drive the chaser to the desired position and attitude quickly. Figs. 5 and 6 show that the estimation error of disturbances and the state of saturation compensator are bounded. The simulation result illustrates that the proposed controller and disturbance observer for the autonomous proximity mission in orbit can guarantee the stability of system, such that the successive docking operation can be effectively achieved.

To show the effectiveness and advantage of the proposed disturbance observer and saturation compensator in (21), the simulation is carried out again without disturbance observation and saturation compensation. Figs. 7 and 8 show the time history of relative position and relative attitude in the absence of disturbance observer (18) and saturation compensator (22). Fig. 9 shows the time history of control forces and torques without the saturation compensation, respectively. By comparing them with Figs. 2–4, we can claim that the proposed robust saturated controller (21) provides a better dynamic performance, which is mainly due to the shorter transient response

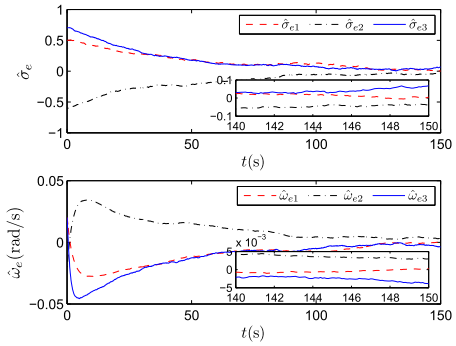

Fig. 8. Response of relative attitude motion without (18) and (22).

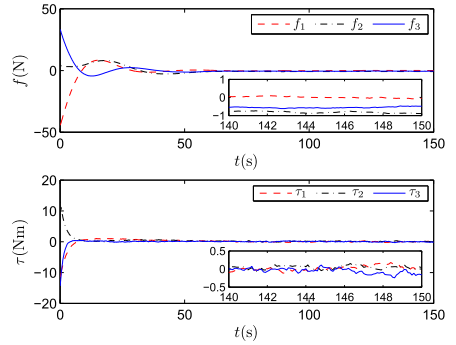

Fig. 9. Response of control forces and control torques without (18) and (22).

time, smaller steady-state errors, and smaller magnitudes of control inputs.

V. Conclusion

An autonomous robust saturated control algorithm has been developed for spacecraft close proximity maneuvers despite of the presence of input saturation effect, parametric uncertainties, measurement uncertainties, kinematic couplings, and unknown external disturbances. The unique feature of this brief lies that the robust saturated control strategy is introduced by the nonlinear state feedback technique with the disturbance observer and saturation compensator, where the disturbance observer is employed to compensate parametric uncertainties, measurement uncertainties, unknown kinematic couplings, and unknown external disturbances. This disturbance observer-based saturated controller appears to be a promising new development for the field of spacecraft autonomous proximity maneuvers. It has been proven that all the signals of the resulting closed-loop system of the 6-DOF relative motion states are uniformly ultimately bounded. The proposed control scheme can drive the chaser to the desired position and attitude precisely, and provide good transient and steady-state performance for the considered close proximity maneuvers. Furthermore, the simulation result on an R-bar proximity scenario has illustrated that the proposed saturated controller is effective and robust to lumped disturbances.

References

[1] J. T.-Y. Wen and K. Kreutz-Delgado, "The attitude control problem," *IEEE Trans. Autom. Control*, vol. 36, no. 10, pp. 1148–1162, Oct. 1991.

[2] D. T. Stansbery and J. R. Cloutier, "Position and attitude control of a spacecraft using the state-dependent Riccati equation technique," in *Proc. Amer. Control Conf.*, Chicago, IL, USA, Jun. 2000, pp. 1867–1871.

[3] N. K. Philip and M. R. Ananthasayanam, "Relative position and attitude estimation and control schemes for the final phase of an autonomous docking mission of spacecraft," *Acta Astronaut.*, vol. 52, no. 7, pp. 511–522, Apr. 2003.

[4] K. Subbarao and S. J. Welsh, "Nonlinear control of motion synchronization for satellite proximity operations," *J. Guid. Control Dyn.*, vol. 31, no. 5, pp. 1284–1294, Sep./Oct. 2008.

[5] J. Liang and O. Ma, "Angular velocity tracking for satellite rendezvous and docking," *Acta Astronaut.*, vol. 69, nos. 11–12, pp. 1019–1028, Dec. 2011.

[6] Z. Meng, W. Ren, and Z. You, "Decentralised cooperative attitude tracking using modified Rodriguez parameters based on relative attitude information," *Int. J. Control*, vol. 83, no. 12, pp. 2427–2439, Dec. 2010.

[7] P. Singla, K. Subbarao, and J. L. Junkins, "Adaptive output feedback control for spacecraft rendezvous and docking under measurement uncertainty," *J. Guid. Control Dyn.*, vol. 29, no. 4, pp. 892–902, Jul./Aug. 2006.

[8] S. B. McCamish, M. Romano, and X. Yun, "Autonomous distributed control of simultaneous multiple spacecraft proximity maneuvers," *IEEE Trans. Autom. Sci. Eng.*, vol. 7, no. 3, pp. 630–644, Jul. 2010.

[9] M. Xin and H. Pan, "Integrated nonlinear optimal control of spacecraft in proximity operations," *Int. J. Control*, vol. 83, no. 2, pp. 347–363, Feb. 2010.

[10] M. Xin and H. Pan, "Indirect robust control of spacecraft via optimal control solution," *IEEE Trans. Aerosp. Electron. Syst.*, vol. 48, no. 2, pp. 1798–1809, Apr. 2012.

[11] S. Di Cairano, H. Park, and I. Kolmanovsky, "Model predictive control approach for guidance of spacecraft rendezvous and proximity maneuvering," *Int. J. Robust Nonlinear Control*, vol. 22, no. 12, pp. 1398–1427, Aug. 2010.

[12] F. Zhang and G. R. Duan, "Integrated translational and rotational finite-time maneuver of a rigid spacecraft with actuator misalignment," *IET Control Theory Appl.*, vol. 6, no. 9, pp. 1192–1204, Jun. 2012.

[13] W.-H. Chen, "Disturbance observer based control for nonlinear systems," *IEEE/ASME Trans. Mechatronics*, vol. 9, no. 4, pp. 706–710, Dec. 2004.

[14] L. Guo and W.-H. Chen, "Disturbance attenuation and rejection for systems with nonlinearity via DOBC approach," *Int. J. Robust Nonlinear Control*, vol. 15, no. 3, pp. 109–125, 2005.

[15] W.-H. Chen, "Nonlinear disturbance observer-enhanced dynamic inversion control of missiles," *J. Guid., Control, Dyn.*, vol. 26, no. 1, pp. 161–166, Jan. 2003.

[16] J. Yang, W.-H. Chen, and S. Li, "Non-linear disturbance observer-based robust control for systems with mismatched disturbances/uncertainties," *IET Control Theory Appl.*, vol. 5, no. 18, pp. 2053–2062, Dec. 2011.

[17] C. Liu, O. McAree, and W.-H. Chen, "Path-following control for small fixed-wing unmanned aerial vehicles under wind disturbances," *Int. J. Robust Nonlinear Control*, vol. 23, no. 15, pp. 1682–1698, Oct. 2013.

[18] S. Li and J. Yang, "Robust autopilot design for bank-to-turn missiles using disturbance observers," *IEEE Trans. Aerosp. Electron. Syst.*, vol. 49, no. 1, pp. 558–579, Jan. 2013.

[19] J. Yang, S. Li, C. Sun, and L. Guo, "Nonlinear-disturbance-observer-based robust flight control for airbreathing hypersonic vehicles," *IEEE Trans. Aerosp. Electron. Syst.*, vol. 49, no. 2, pp. 1263–1275, Apr. 2013.

[20] Q. Hu, B. Li, and J. Qi, "Disturbance observer based finite-time attitude control for rigid spacecraft under input saturation," *Aerosp. Sci. Technol.*, vol. 39, pp. 13–21, Dec. 2014.

[21] S. N. Wu, X. Y. Sun, Z. W. Sun, and X. D. Wu, "Sliding-mode control for staring-mode spacecraft using a disturbance observer," *Proc. Inst. Mech. Eng., G, J. Aeros. Eng.*, vol. 224, no. G2, pp. 215–224, 2010.

[22] B. Cong, Z. Chen, and X. Liu, "Disturbance observer-based adaptive integral sliding mode control for rigid spacecraft attitude maneuvers," *Proc. Inst. Mech. Eng., G, J. Aeros. Eng.*, vol. 227, no. 10, pp. 1660–1671, Oct. 2013.

[23] L. Sun and W. Huo, "Robust adaptive relative position tracking and attitude synchronization for spacecraft rendezvous," *Aerosp. Sci. Technol.*, vol. 41, pp. 28–35, Feb. 2015.

[24] L. Sun and W. Huo, "6-DOF integrated adaptive backstepping control for spacecraft proximity operations," *IEEE Trans. Aerosp. Electron. Syst.*, vol. 51, no. 3, pp. 2433–2443, Jul. 2015.

[25] L. Sun and W. Huo, "Adaptive fuzzy control of spacecraft proximity operations using hierarchical fuzzy systems," *IEEE/ASME Trans. Mechatronics*, vol. 21, no. 3, pp. 1629–1640, Jun. 2016.

[26] H. Schaub and J. L. Junkins, *Analytical Mechanics of Space Systems*. Reston, VA, USA: AIAA, 2003.
[27] M. Xin and H. Pan, "Nonlinear optimal control of spacecraft approaching a tumbling target," *Aerosp. Sci. Technol.*, vol. 15, no. 2, pp. 79–89, Mar. 2011.
[28] M. D. Shuster, "A survey of attitude representations," *J. Astron. Sci.*, vol. 41, no. 4, pp. 439–517, Oct./Nov. 1993.
[29] S. Segal, A. Carmi, and P. Gurfil, "Stereovision-based estimation of relative dynamics between noncooperative satellites: Theory and experiments," *IEEE Trans. Control Syst. Technol.*, vol. 22, no. 2, pp. 568–584, Mar. 2014.
[30] P. Z. Schulte and D. A. Spencer, "Development of an integrated spacecraft guidance, navigation, & control subsystem for automated proximity operations," *Acta Astronaut.*, vol. 118, pp. 168–186, Jan./Feb. 2016.
[31] A. H. J. de Ruiter, "Observer-based adaptive spacecraft attitude control with guaranteed performance bounds," *IEEE Trans. Autom. Control*, vol. 61, no. 10, pp. 3146–3151, Oct. 2016.
[32] C. Wen and P. Gurfil, "Guidance, navigation and control for autonomous R-bar proximity operations for geostationary satellites," *Proc. Inst. Mech. Eng., G, J. Aeros. Eng.*, vol. 231, no. 3, pp. 452–473, Mar. 2017.
[33] J. N. Yun, J. Su, Y. I. Kim, and Y. C. Kim, "Robust disturbance observer for two-inertia system," *IEEE Trans. Ind. Electron.*, vol. 60, no. 7, pp. 2700–2710, Jul. 2013.
[34] L. Wang and J. Su, "Robust disturbance rejection control for attitude tracking of an aircraft," *IEEE Trans. Control Syst. Technol.*, vol. 23, no. 6, pp. 2361–2368, Nov. 2015.